Research on Chemical Intermediates
https://doi.org/10.1007/s11164-021-04439-1

Basic ionic liquid anchored on UiO-66-NH_2 metal–organic framework: a stable and efficient heterogeneous catalyst for synthesis of xanthenes

Saeed Askari[1] · Mohammad Mehdi Khodaei[1,2] · Mohammad Jafarzadeh[1,2]

Received: 11 December 2020 / Accepted: 25 March 2021

Abstract

In this study, the Zr-based metal–organic framework, UiO-66-NH_2, was modified with ionic liquid (dibutylimidazolium bromide) to generate a platform for supporting an organocatalyst of guanidine. After an anion exchange, the prepared hybrid system was denoted as UiO-66-NH_2-$ILPF_6^-$-guanidine. The catalyst was characterized by different techniques such as PXRD, FTIR, TEM, SEM–EDS, TGA, and BET. The basic heterogeneous catalyst was then utilized for the synthesis of xanthene derivatives via a reaction of aldehydes with dimedone. Various types of aromatic aldehydes were employed for the synthesis with medium to high yield. The study of catalytic activities showed that the heterogenization of guanidine significantly promotes catalytic performance in comparison with guanidine in a homogeneous form. The heterogeneous catalyst is stable in the reaction medium and can be recycled for at least four times without significant reduction in activity. The stability of the catalyst was also investigated by XRD, FTIR, SEM/elemental mapping, and leaching test.

Keywords Heterogeneous catalyst. · Metal–organic framework. · Ionic-liquid. Guanidine. · Xanthene

✉ Mohammad Mehdi Khodaei
mmkhoda@razi.ac.ir

✉ Mohammad Jafarzadeh

[1] Department of Organic Chemistry, Razi University, 67149-67346 Kermanshah, Iran

[2] Nanoscience & Nanotechnology Research Center (NNRC), Razi University, 67149-67346 Kermanshah, Iran

Published online: 01 April 2021

Introduction

A vast application of ionic liquids (ILs) in science and technology is related to their interesting behaviors of high polarity, non-volatility, high thermal stability, high conductivity, and a large variety of components in their structures [1]. Their applications in catalysis have boomed with the introduction and development of Task-Specific ILs (TSILs) [2]. Numerous organic reactions were carried out by applying TSILs. Recyclability, reusability, and leaching of TSILs are major concerns in the development of these materials for industrial applications. By heterogenization of ILs to porous solid supports (e.g., polymer, silica, MCM-41, SBA-15, metal oxides, MOFs), generation of supported ILs (SILs), the physicochemical properties of ILs transfer to the support [3]. Besides a synergic effect between IL and support, the recyclability can be promoted and the leaching minimized [4, 5].

Metal–organic frameworks (MOFs) are composed of metallic oxides (nodes) and bi-/multi-functional ligands. Their reticular structures provide high crystallinity, high porosity (large surface area, micro/mesopores, large pore volume), tunable synthetic methods, reasonable chemical/thermal stabilities with a broad range of applications, mainly gas adsorption [6], catalysis [7–10], drug delivery [11–13], etc. MOFs could use as catalysts individually (metal node as a Lewis acid site) [14–17] and being a support for metallic [18, 19], organometallic [20, 21], and organic [22, 23] catalytic systems. MOFs have been also used as support for ILs (i.e., SILs), particularly TSILs [24]. ILs could either confine in MOF pores [25] or covalently attached to the MOF nodes/ligands [4]. MOF-supported ILs have been found in many applications in the synthesis of a large variety of organic compounds [26–32]. As follow, we describe the application of the selected catalytic systems reported recently. Chong et al. used 1-butyl-3-methylimidazolium bromide (BmimBr)/NH_2-MIL-101(Cr) for the synthesis of *N*-aryl oxazolidin-2-ones from carbon dioxide and epoxides, via confinement of the IL in the MOF pores [33]. The catalyst was recycled and reused and showed a synergic effect of the IL and the MOF. Jin et al. reported a catalytic system of IL/polyoxometalate@MOF for epoxidation of cycloolefins with H_2O_2 [34]. A synergistic effect between 1-octyl-3-methylimidazolium bromide, $PMo_{10}V_2$, and MIL-100(Fe) was observed by activation of POM with imidazolium cations of the IL. Chen et al. reported [HVIm-$(CH_2)_3SO_3H$]HSO_4@HKUST-1(Cu) catalyst, with available Lewis and Brønsted acid sites, for esterification of oleic acid [35].

Xanthenes, with an oxygen-containing ring in the core, can be found in compounds with biological activities (e.g., antiviral, antibacterial), fluorescent dyes for applications in laser technology and sensing [36], and used as a corrosion inhibitor [37]. They can be prepared by reaction of aryl aldehydes or aromatic hydroxyls (e.g., â-naphthol) with dimedone (i.e., 5,5-dimethyl-cycloheaxan-1,3-dione) in the presence of acidic [36, 38], basic, and metallic [39] catalysts under conventional, solvent-free [40], microwave [41] and ultrasonic [42] conditions. Various catalytic systems were introduced in the literature such as $CoFe_2O_4$/OCMC/Cu(BDC) [43], L-Proline [44], $Cu(OAc)_2$ [45], cyclodextrin/

melamine/Ag [46], Fe-Cu/ZSM-5 [47], MWCNs/$Ru(CO)_4$ [48], $NiFe_2O_4$@Cu/montmorillonite [49], $ZnCl_2$/urea as a deep eutectic solvent (DES) [50], cerium (IV) ammonium nitrate/ultrasonic [51], 1,1´-butylenebis(3-sulfo-3*H*-imidazol-1-ium) chloride as a binuclear TSIL [52], [(*n*-propyl)$_2NH_2$][HSO_4^-] [53] and perlite nanoparticles@IL/$ZrCl_4$ [54]. Most recently, Lewis acid sites in MOFs (i.e., Cu/Cr-MIL-101) catalyzed the reaction to xanthenes [55]. The bimetallic MOFs showed a synergic effect with higher catalytic activity compared to the corresponding MOFs, Cu-BDC and Cr-MIL-101, individually. Abo El-Yazeed and co-workers employed a bimetallic Fe–Mg MOF for the catalytic synthesis of xanthenes [56]. Core–shell nanoparticle-supported imidazolium IL (i.e., Fe_3O_4@propylsilane-histidine[HSO_4^-]) was introduced for the synthesis of xanthene derivatives [57]. Zwitterionic and ionic structures, 4-[3-(4-sulfo-butyl)-imidazol-1-yl]-butane-1-sulfonate and 4-imidazol-1-yl-butane-1-sulfonate imidazolium, were also used for the synthesis of xanthenes [58].

Recently, we have immobilized butylimidazolium IL to a zirconium-based MOF, UiO-66-NH_2, with a subsequent functionalization of the IL using urea [59]. The basic IL was used for the synthesis of oximes. Since guanidine is recognized as a base catalyst, which has been used recently for transesterification to biodiesel [60], it was used for the functionalization of UiO-66-NH_2-supported butylimidazolium in this study. The UiO-66-NH_2-ILPF_6^--guanidine as a heterogeneous catalyst was then used for the base-catalyzed synthesis of xanthenes. The effect of solvent type, temperature, catalyst amount, and catalyst recoverability, and reusability were studied.

Experimental

Material and physical measurements

The materials were purchased from Merck and used without any additional purification. Powder X-ray diffraction (XRD) was conducted by a Philips PW1730 diffractometers (Cu K_α, $\lambda = 1.5418$ Å). Infrared spectra were recorded with FT-IR spectrometer (WGH-30/6300), in the range of 400–4000 cm^{-1}. Transmission electron microscopy (TEM) images were obtained using a Philips EM 208S instrument at an accelerating voltage of 100 kV. Field emission scanning electron microscopy (FESEM, Model: TESCAN MIRA3) and energy-dispersive spectroscopy (EDS) were used for morphological and compositional studies, respectively. Thermogravimetric analysis (TGA, model: Q600) was carried out at the heating rate of 7 °C min^{-1} under nitrogen flow. The BET surface area and pore volume were measured by a Belsorp mini II porosimeter. The metal content was determined by inductively coupled plasma-optical emission spectroscopy (ICP-OES, model: Perkin-Elmer DV5300). The organic products were characterized by ^1H and ^{13}C nuclear magnetic resonance (NMR, Model: Bruker AVANCE 300 MHz) spectroscopy.

Preparation of UiO-66-NH_2-$ILBr^-$

1,3-Bis-(4-bromobutyl)-3*H*-imidazol-1-ium bromide ($ILBr^-$) was initially prepared according to our reported method [59]. The preparation of UiO-66-NH2 was carried out by adopting a method reported in the literature [61]. For the preparation of immobilized IL on the MOF, UiO-66-NH2 (0.1 g) was dispersed in 10 mL DMF under ultrasonic irradiation and $ILBr^-$ (0.03 mmol, 0.01 g) was then added, which was stirred at room temperature for 24 h.

Preparation of UiO-66-NH_2-$ILBr^-$-guanidine

Guanidine hydrochloride (0.06 mmol, 0.005 g) was added to UiO-66-NH_2-$ILBr^-$ (0.1 g) dispersed in 10 mL DMF and stirred at room temperature for 24 h. The product (UiO-66-NH2-$ILBr^-$-guanidine) was isolated by centrifugation, washed with DMF and ethanol several times, and dried at 80 °C in an oven for 24 h.

Preparation of UiO-66-NH_2-$ILPF_6^-$-guanidine

The Br^- counter anion was exchanged with hexafluorophosphate (PF_6^-) using potassium hexafluorophosphate (0.75 mmol, 0.138 g) in acetone (2 mL) under stirring at room temperature for 24 h. The final product (UiO-66-NH2-$ILPF_6^-$-guanidine) was filtered, washed with H_2O (3 × 10 mL), EtOH (3 mL), Et_2O (2.5 mL), acetone (2.5 mL), and dried at 50 °C in an oven overnight.

Typical procedure for the synthesis of 3,3,6,6-tetramethyl-9-phenyl-3,4,5,6-tetrahydro-9H-xanthene

UiO-66-NH_2-$ILPF_6^-$-guanidine (0.03 g) dispersed in 1 mL ethanol was added to a mixture of benzaldehyde (1 mmol, 0.11 mL) and dimedone (2 mmol, 0.280 g). The mixture was stirred at room temperature at an appropriate time to complete the reaction. The reaction progress was monitored by TLC. After completion of the reaction, the catalyst was separated from the reaction medium by centrifugation, washed with ethanol, and dried in an oven (70 °C) overnight. The organic products were isolated from the reaction mixture with the evaporation of the solvent and then purified by recrystallization. The xanthene derivatives were identified by ^1H and ^{13}C NMR (300 and 75 MHz, respectively). The catalyst was also reused several times.

The spectral data for the selected products

3,4,6,7-Tetrahydro-9-(4-methoxyphenyl)-3,3,6,6-tetramethyl-2*H*-xanthene-1,8-(5*H*,9*H*)-dione (Fig. S1)

^1H NMR (300 MHz, $CDCl_3$); δ (ppm) = 1.02 (s, 6H, 2 × CH_3), 1.11 (s, 6H, 2 × CH_3), 2.23 (q, 4H, 2 × CH_2), 2.49 (s, 4H, 2 × CH_2), 3.74 (s, 3H, OCH_3), 4.70 (s, 1H, CH), 6.73 (d, 2H, J = 6.75 Hz, Ar–H), 7.28 (d, 2H, J = 7.25 Hz, Ar–H); ^{13}C NMR

(75 MHz, $CDCl_3$): δ (ppm) = 27.4, 29.8, 30.9, 32.3, 40.6, 50.8, 115.2, 116.0, 129.3, 135.3, 154.6, 162.4, 197.5.

3,4,6,7-Tetrahydro-9-(4-hydroxyphenyl)-3,3,6,6-tetramethyl-2*H*-xanthene-1,8-(5*H*,9*H*)-dione (Fig. S2)

^{1}H NMR (300 MHz, $CDCl_3$); δ (ppm) = 1.02 (s, 6H, 2 × CH_3), 1.13 (s, 6H, 2 × CH_3), 2.22 (q, 4H, 2 × CH_2), 2.48 (s, 4H, 2 × CH_2), 3.76 (s, 1H, OH), 4.73 (s, 1H, CH), 6.5 (d, 2H, *J* = 6.58 Hz, Ar–H), 7.0 (d, 2H, *J* = 7.09 Hz, Ar–H); ^{13}C NMR (75 MHz, $CDCl_3$): δ (ppm) = 27.10, 29.43, 30.57, 32.01, 40.61, 51.01, 55.04, 113.16, 116.03, 136.50, 158.06, 162.08, 196.64.

3,4,6,6-Tetramethyl-9-phenyl-3,4,5,6,7,9-hexahydro-1*H*-xanthene-1,8(2*H*)-dione (Fig. S3)

^{1}H NMR (300 MHz, $CDCl_3$); δ (ppm) = 1.13 (s, 6H, 2 × CH_3), 1.27 (s, 6H, 2 × CH_3), 2.20 (s, 4H, 2 × CH_2), 2.42 (q, 4H, 2 × CH_2), 5.58 (s, 1H, CH), 7.11–7.22 (m, 5H); ^{13}C NMR (75 MHz, $CDCl_3$): δ (ppm) = 27.1, 29.6, 31.4, 32.6, 46.1, 47.5, 115.5, 125.6, 126.9, 128.4, 137.5, 159.0, 189.2.

3,3,6,6-Tetramethyl-9-(3-nitrophenyl)-3,4,5,6,7,9-hexahydro-1*H*-xanthene-1,8(2*H*)-dione (Fig. S4)

^{1}H NMR (300 MHz, $CDCl_3$); δ (ppm) = 1.15 (s, 6H, 2 × CH_3), 1.30 (s, 6H, 2 × CH_3), 2.40–2.48 (m, 4H, 2 × CH_2), 2.48–2.56 (m, 4H, 2 × CH_2), 5.61 (s, 1H, CH), 7.21–8.06 (m, 4H); ^{13}C NMR (75 MHz, $CDCl_3$): δ (ppm) = 27.4, 29.5, 31.2, 32.9, 46.6, 47.0, 114.9, 121.2, 122.1, 129.1, 133.3, 140.8, 148.5, 189.7.

Results and discussion

Preparation and characterization of UiO-66-NH_2-ILPF_6^--guanidine

The preparation steps of UiO-66-NH_2-ILPF_6^--guanidine are summarized in Scheme 1. Initially, the ILBr^- was prepared according to our previously reported method [59] and then immobilized on the surface of UiO-66-NH_2 by post-synthesis modification (PSM) method. Guanidine hydrochloride was attached to the supported ionic liquid (UiO-66-NH_2-ILBr^-) and the Br^- was then exchanged by PF_6^- to finally generate supported ionic liquid catalyst (SILC). The prepared catalyst, UiO-66-NH_2-ILPF_6^--guanidine, was characterized by different techniques including XRD, FT-IR, TEM, SEM–EDS, TGA, and BET.

To evaluate the crystal stability of UiO-66-NH_2 after the introduction of IL, powder XRD was used over the diffraction angle (2θ) of 5–80° (Fig. 1). The characteristic diffractions of the UiO-66-NH_2 were found to be almost similar to the pattern of that framework in the literature [62]. The diffractions at angles of 7.6°, 7.9°, 14°, 16.4°, 21.4°, 24.8°, 29.8°, 32.2°, 34.9°, 36.8°, 40.1°, 42.7°, 49.3°, and

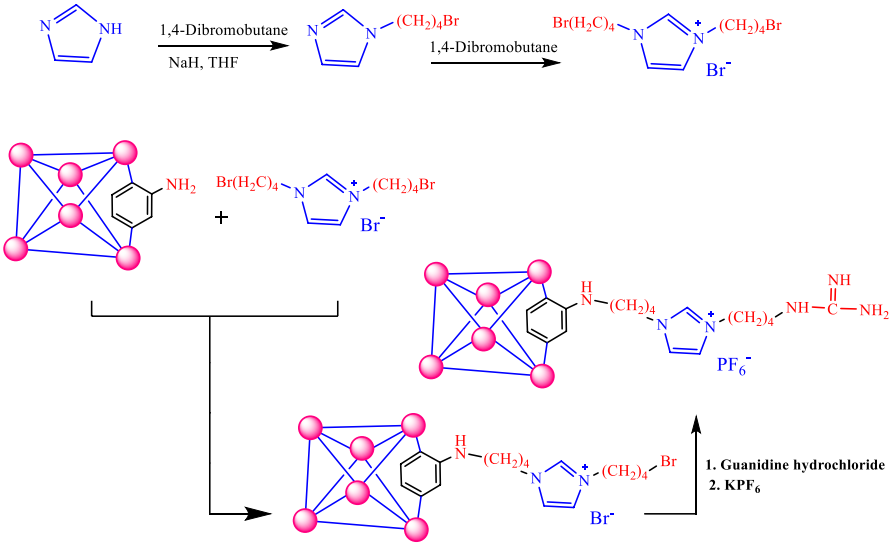

Scheme 1 Preparation of $ILBr^-$ and UiO-66-NH_2-$ILPF_6^-$-guanidine

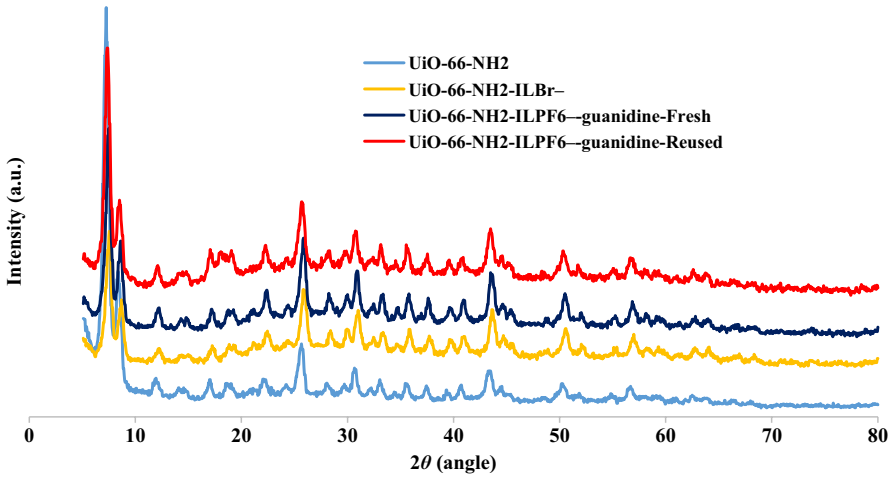

Fig. 1 XRD patterns of UiO-66-NH_2, UiO-66-NH_2-$ILBr^-$, and UiO-66-NH_2-$ILPF_6^-$-guanidine (fresh and reused)

55.9° were observed corresponding to the (111), (200), (222), (400), (511), (600), (711), (731), (820), (751), (664), (933), (955), and (12 42) planes, respectively. For UiO-66-NH_2-$ILBr^-$ and UiO-66-NH_2-$ILPF_6^-$-guanidine, similar patterns to the pattern of UiO-66-NH_2 were observed indicating the structural preservation of the MOF framework during PSM with IL and the attachment of guanidine. A slight reflection shift, corresponding to the angles of 7.6°, 7.9°, 24.8°, and 43.7°, toward higher angles was observed for the functionalized MOF with IL (Fig. S5).

It indicates that the ILs on the surface compress the flexible framework of the MOF to form a smaller unit cell.

Post-synthetic modification of the UiO-66-NH_2 with $ILBr^-$ was further confirmed by FT-IR spectroscopy. The FT-IR spectra of UiO-66-NH_2, UiO-66-NH_2-$ILBr^-$ and UiO-66-NH_2-$ILPF_6^-$-guanidine are presented in Fig. 2. The stretching peaks at 3460 and 3336 cm^{-1} are attributed to the NH_2 band of primary amine, which indicates the presence of the amine group within the framework of UiO-66-NH_2 [61]. The stretching peaks at 1573, 1496, 1253, and 600–750 cm^{-1} are assigned to C = C (aromatic ring), C-N (C-NH_2), and Zr-O bonds of UiO-66-NH_2, respectively [62]. After modification, the C-NH_2 band of a primary amine was converted to C-NH of a secondary amine and the stretching vibration of the NH bond appeared at 3452 cm^{-1}. The observed band at 1654 cm^{-1} is related to stretching vibration of C = N of imidazolium ring, and the stretching band at 663 cm^{-1} is corresponded to CH_2-Br which overlapped with the UiO-66-NH_2 peaks. These results confirmed the incorporation of $ILBr^-$ to UiO-66-NH_2. Finally, the binding of guanidine to the ionic liquid results in the formation of two bands at 3452 and 3334 cm^{-1}, which are corresponded to NH_2 of guanidine.

The morphology of UiO-66-NH_2 and UiO-66-NH_2-$ILPF_6^-$-guanidine was investigated by TEM and SEM (Fig. 3). The TEM images of UiO-66-NH_2 and UiO-66-NH_2-$ILPF_6^-$-guanidine show that the MOF particles were aggregated, and the size of aggregated particles was found to be in the range of ~ 50–100 nm. The SEM images show irregular and spherical shapes for UiO-66-NH_2 and UiO-66-NH_2-$ILPF_6^-$-guanidine, respectively. The EDS spectrum of UiO-66-NH_2-$ILPF_6^-$-guanidine confirmed the presence of corresponding elements of the

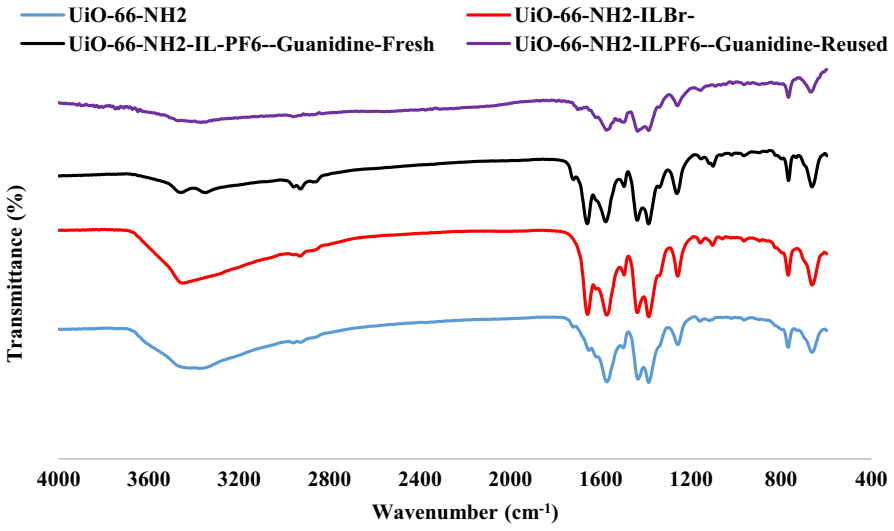

Fig. 2 FT-IR spectra of UiO-66-NH_2, UiO-66-NH_2-$ILBr^-$,UiO-66-NH_2-IL $ILPF_6^-$-guanidine (fresh and reused)

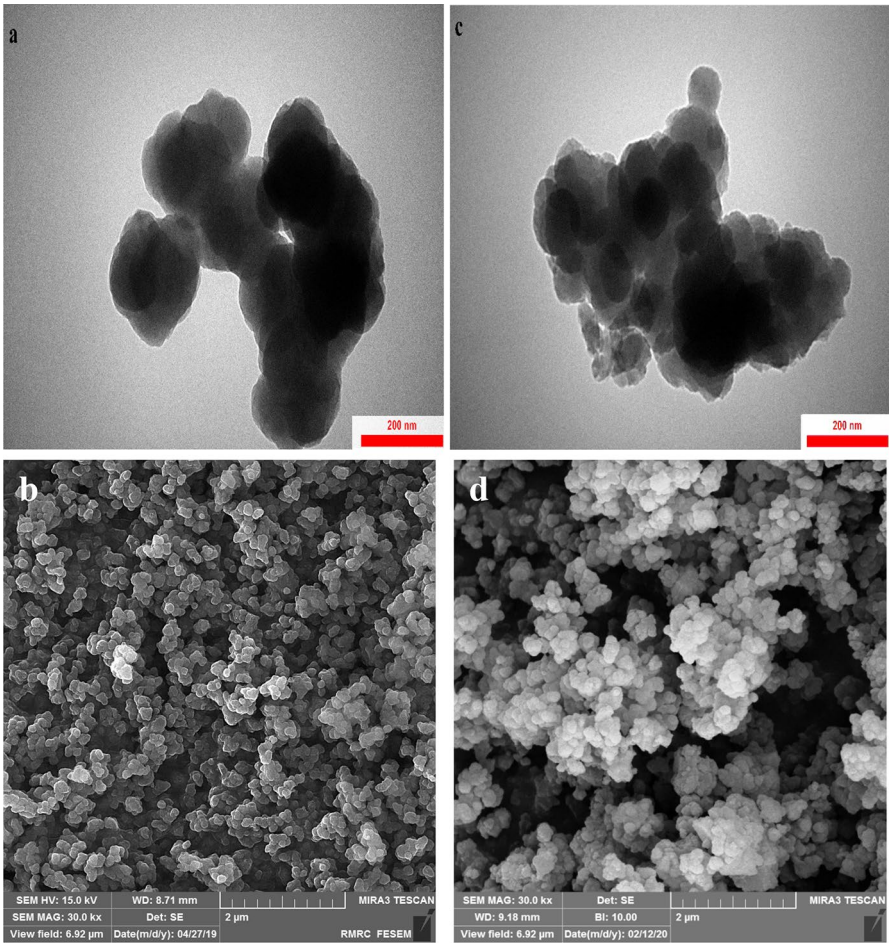

Fig. 3 TEM and SEM images of (a,b) UiO-66-NH_2 and (c,d) UiO-66-NH_2-$ILPF_6^-$-guanidine

framework, IL, and guanidine (Fig. 4). The elemental mapping demonstrated that the elements were distributed homogeneously in the structure.

The thermal behavior of UiO-66-NH_2-$ILPF_6^-$-guanidine was investigated by thermogravimetric analysis and three steps of weight loss observed (Fig. 5). In the first step, a weight loss of ~ 20% was found in the temperature range of 25–140 °C, attributed to physically adsorbed solvents (i.e., DMF and ethanol) and moisture in the pores. The second step in the temperature range of 140–470 °C was observed with ~ 14.7% weight loss, related to the removal of coordinated DMF from the framework, degradation of IL and guanidine, and the partial degradation of the MOF frameworks [63]. The content of $ILBr^-$ was estimated at ~ 6.3% by comparison of the second step weight losses of UiO-66-NH_2 and UiO-66-NH_2-$ILBr^-$ according to our previous report [59]. We are expecting that a part of IL has been functionalized by guanidine. The decomposition of the entire

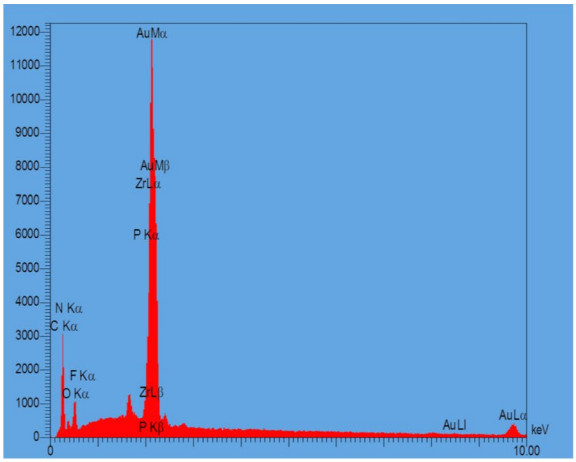

Element	wt. %	at. %
C	19.06	50.31
F	3.22	5.36
Zr	16.56	4.42
O	10.46	20.73
P	5.82	5.95
N	3.69	8.35

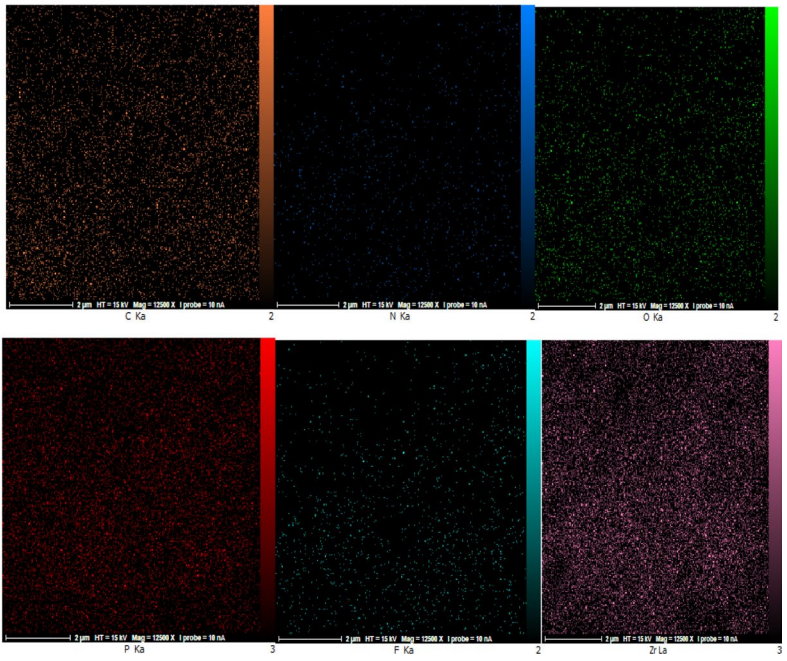

Fig. 4 EDS spectrum and elemental mapping of the UiO-66-NH_2-$ILPF_6^-$-guanidine (fresh)

framework occurred in the third step at a temperature above 470 °C with a weight loss of ~ 9.9%.

Figure 6 shows the N_2 adsorption/desorption isotherms and the corresponding pore size distributions of UiO-66-NH_2 and UiO-66-NH_2-$ILPF_6^-$-guanidine. The pattern of isotherms is consistent with the gas sorption behavior of microporous materials (type I) [64]. The data of the surface area and the porosity are given in Table 1. As expected, the BET specific surface area and total pore volume of the

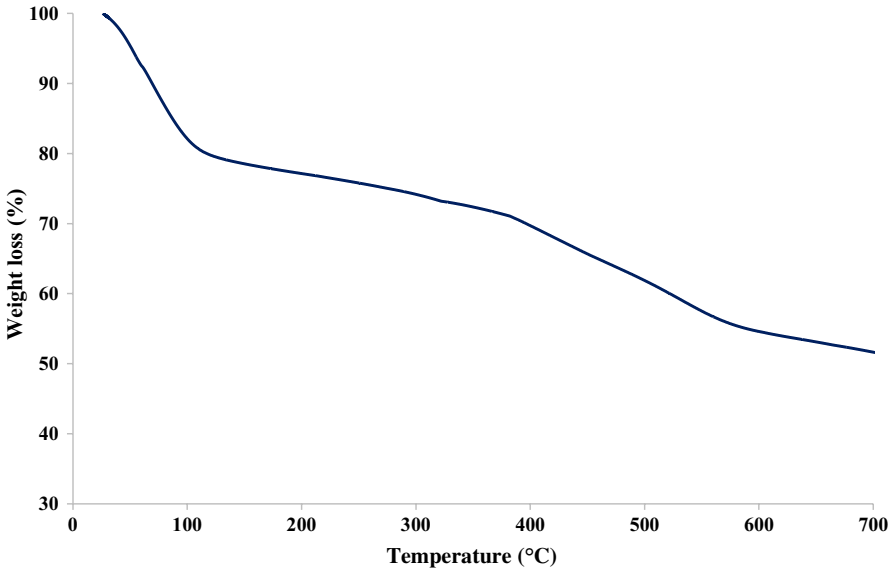

Fig. 5 TGA thermogram of UiO-66-NH_2-$ILPF_6^-$-guanidine

UiO-66-NH_2 decreased after functionalization with IL and guanidine. The pore size of UiO-66-NH_2-$ILPF_6^-$-guanidine was found to be the same as that in UiO-66-NH_2, which is consistent with the pore size distribution curves. The high surface area of the catalyst provides a high number of the available active sites on the surface to interact with reactants. Moreover, the large pore volume facilitates easy access to the pore interior for efficient contact between the reactants and the catalyst active sites.

The catalytic activity of the catalyst

The catalytic performance of the UiO-66-NH_2-$ILPF_6^-$-guanidine was evaluated in the synthesis of xanthenes. A model reaction, using benzaldehyde (1 mmol) and dimedone (2 mmol) as precursors, was chosen to find the optimum conditions by considering solvent type, temperature, and catalyst amount. The results of optimal conditions are presented in Table 2. Various solvents such as CH_2Cl_2, CH_3CN, H_2O, EtOH, and EtOH:H_2O (1:1) were used for the reaction. Solvents with medium polarity (Table 2, entries 3, 5, 6) exhibited better performance for the synthesis compared to a non-polar solvent (CH_2Cl_2) and a solvent with high polarity (H_2O). The highest reaction efficiency was obtained by utilizing EtOH; a suitable medium for the reaction components. In contrast, the lowest yield of 33% was observed in the absence of solvent. In other words, the solvent is vital for the efficient contacts of the precursors. The effect of elevated temperature on the reaction efficiency was examined (Table 2, entries 6–8). It was found that the reaction efficiency decreased by increasing the reaction temperature to 60 and 80 °C. The same phenomenon has been observed in our previous work

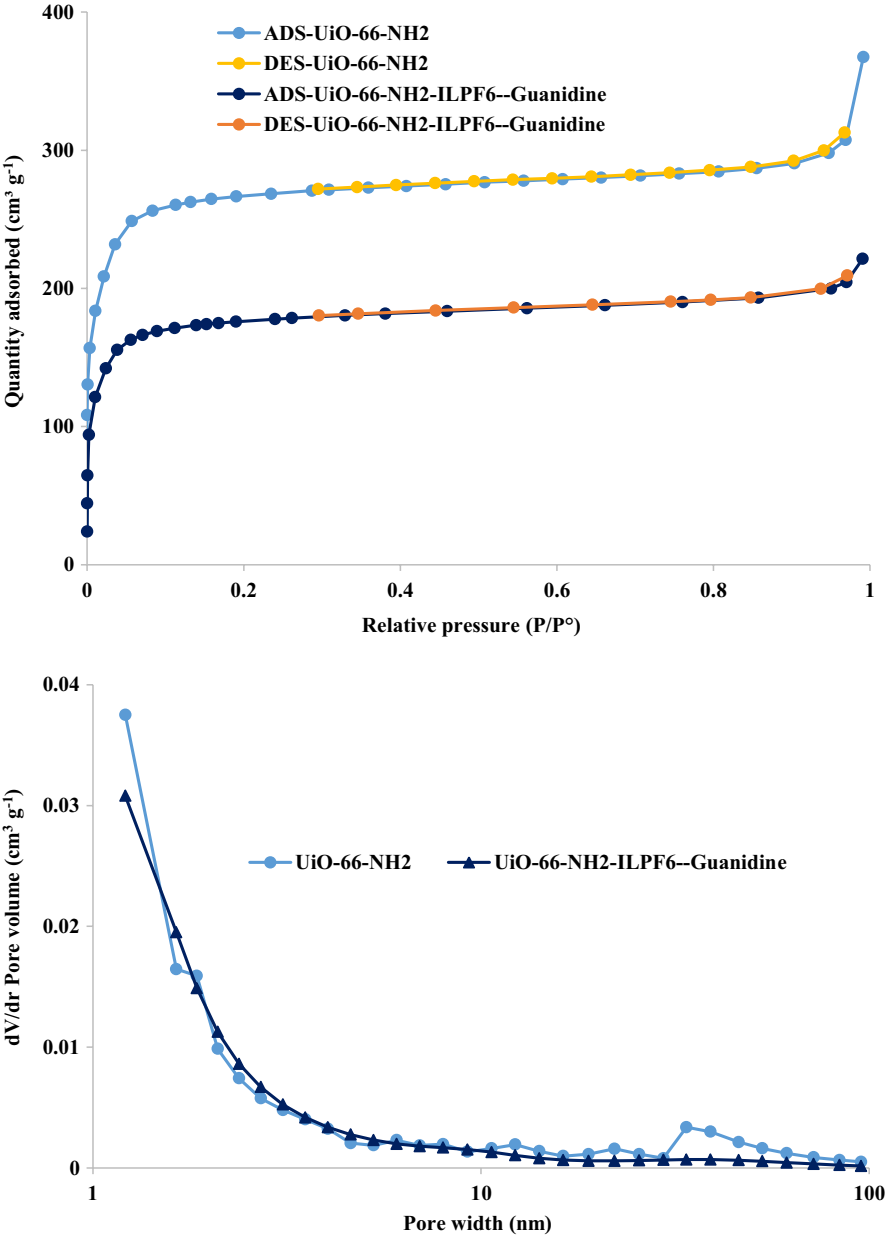

Fig. 6 N_2 adsorption–desorption isotherms and the corresponding pore size distribution curves of UiO-66-NH_2 and UiO-66-NH_2-$ILPF_6^-$-guanidine

using MOF/$ILBF_4^-$/Urea catalyst in the synthesis of oximes [59]. However, the room temperature was chosen for further study (Table 2, entry 6). The quantity of the catalyst was studied, and the results showed that by increasing the catalyst

Table 1 The surface area and the porosity data for UiO-66-NH_2 and UiO-66-NH_2-$ILPF_6^-$-guanidine

Materials	Specific surface area (m^2g^{-1})[a]	Total pore volume (cm^3g^{-1})[b]	Mean pore size (nm)[c]
UiO-66-NH_2	1072	0.56	2.09
UiO-66-NH_2-$ILPF_6^-$-guanidine	648	0.34	2.10

[a]S_{BET}

[b]Total pore volume determined at $P/P_0 = 0.99$

[c]Mean pore diameter determined using the BJH method

Table 2 Optimization of the reaction conditions[a]

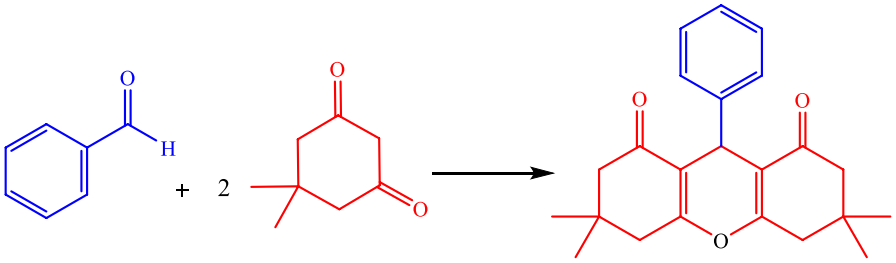

Entry	Solvent	Catalyst amount (g)	Temperature (°C)	Yield (%)[b]
1	Solvent-Free	0.03	25	33
2	CH_2Cl_2	0.03	25	45
3	CH_3CN	0.03	25	70
4	H_2O	0.03	25	55
5	EtOH: H_2O (1:1)	0.03	25	65
6	EtOH	0.03	25	95
7	EtOH	0.03	60	95
8	EtOH	0.03	80	95
9	EtOH	0.05	25	95
10	EtOH	0.1	25	95

[a]Reaction conditions: benzaldehyde (1 mmol), dimedone (2 mmol), solvent (1 mL), UiO-66-NH_2-$ILPF_6^-$-guanidine, 45 min

[b]Isolated yield

Table 3 Synthesis of xanthenes via reactions of aldehydes with dimedone

Entry	Aldehydes	Yield (%)[a]	Time (min)	m.p. (°C) found	m.p. (°C) reported
1	C_6H_5CHO	95	45	194–198	202–204 [65]
2	4-OMe-C_6H_4CHO	93	50	136–140	138 [66]
3	4-Me-C_6H_4CHO	92	60	128–132	132–133 [65]
4	4-OH-C_6H_4CHO	94	55	190–192	194–196 [67]
5	4-Cl-C_6H_4CHO	82	50	228–232	230–232 [65]
6	2,4-Cl_2-C_6H_3CHO	85	55	196–200	197–199 [66]
7	4-NO_2-C_6H_4CHO	95	45	188–192	192–194 [66]
8	3-NO_2-C_6H_4CHO	90	45	166–170	166–168 [68]

Reaction conditions: aldehyde (1 mmol), dimedone (2 mmol), ethanol (1 mL), UiO-66-NH_2-$ILPF_6^-$-guanidine (0.03 g), rt

[a]Isolated yield

content from 0.03 to 0.05 and 0.1, the efficiency of the reaction did not change (Table 2, entries 6, 9, 10). Therefore, the best conditions for the reaction were found by employing ethanol, room temperature, and 0.03 g of the catalyst.

To examine the capability of various aldehydes in the synthesis of xanthenes, aromatic aldehydes were used to react with dimedone (Table 3). Aryl aldehydes with electron-donating and electron-withdrawing groups, including –OMe, –Me, –OH, –Cl, and –NO_2, exhibited high yields in the optimized reaction conditions. In other words, the nature of the substituent did not affect significantly the efficiency of the reaction.

The type of catalyst was another effective parameter on reaction efficiency (Table 4). The support (i.e., UiO-66-NH_2) and the IL (in the homogeneous form) were less reactive in the synthesis, while guanidine and $ILPF_6^-$/guanidine, both in homogeneous form, exhibited relatively good yields. Although $ILPF_6^-$/guanidine showed a slightly higher yield than guanidine hydrochloride, the synergistic effect between IL and guanidine was not significant. Since the high surface area and

Table 4 The catalytic activity of the catalyst, the support, and the ILs (in homogeneous phase)

Entry	Catalyst	Time (min)	Yield (%)[a]
1	UiO-66-NH_2-$ILPF_6^-$-guanidine	45	95
2	UiO-66-NH_2-$ILBr^-$-guanidine	60	80
3	UiO-66-NH_2	90	35
4	$ILBr^-$	120	Trace
5	$ILPF_6^-$	120	25
6	$ILPF_6^-$-guanidine	60	73
7	Guanidine hydrochloride	60	70

Reaction conditions: benzaldehyde (1 mmol), dimedone (2 mmol), ethanol (1 mL), catalyst (0.03 g), rt

[a]Isolated yield

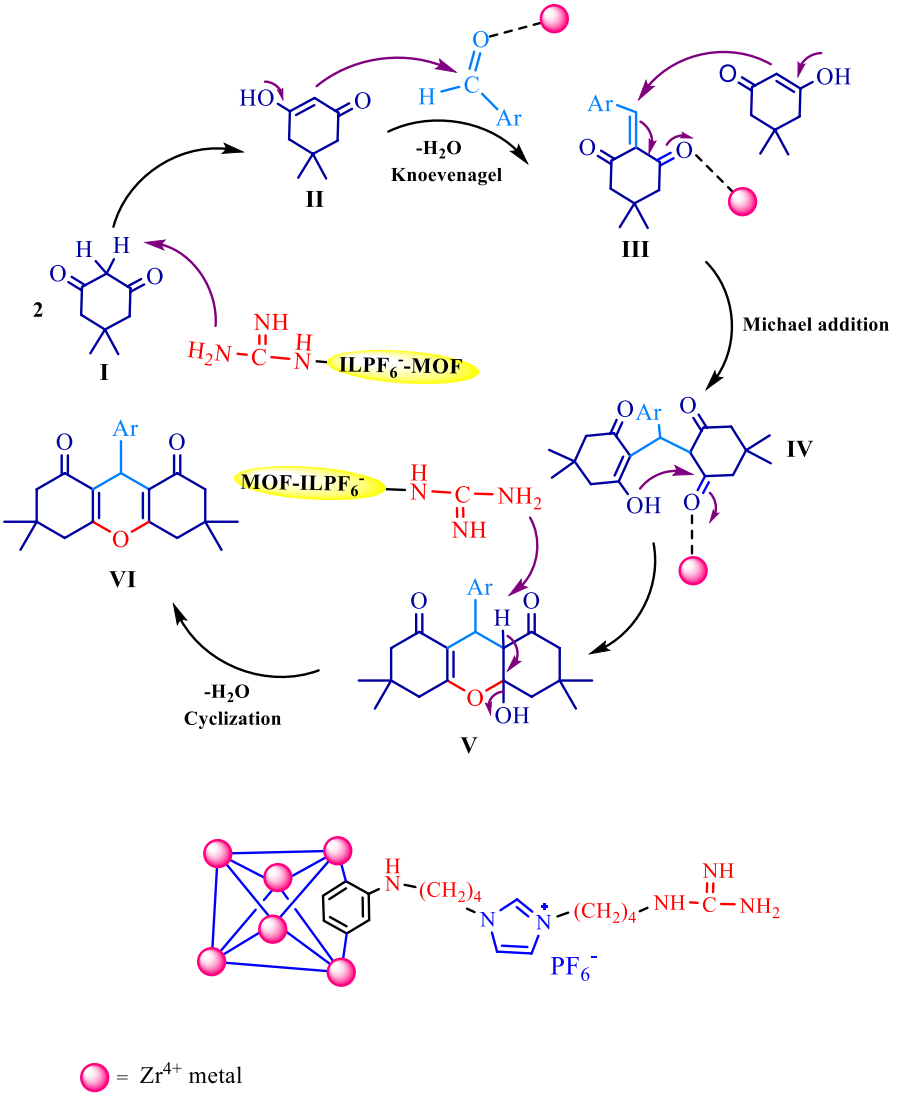

Fig. 7 The proposed mechanism for the synthesis of xanthenes using UiO-66-NH_2-$ILPF_6^-$-guanidine

porosity of the support provide a high number of active sites for immobilizing IL and then guanidine, therefore higher performance was observed for the supported catalyst (Table 4, entries 1 and 2). In other words, a synergistic effect was observed between the support and the IL/guanidine. Furthermore, the type of counter anion of the IL was found to be effective on the reaction yield, as $ILPF_6^-$ (Table 4, entries 1 and 5) showed higher activity than $ILBr^-$ (Table 4, entries 2 and 4).

The mechanism of the synthesis of xanthenes involves a tandem reaction of Knoevenagel, Michael, and intramolecular cyclization catalyzed by a base (Fig. 7) [39]. The supported guanidine plays the role of the base in deprotonation of the acidic proton of the dimedone, while the metallic nodes of the MOF activate the carbonyl of aldehydes. In addition, the supported IL can polarize the area near the surface of the catalyst and facilitate the contact of the starting materials and the catalyst surface.

Reusability of the catalyst

After completion of the reaction under optimized reaction conditions, the catalyst was recycled by filtration, washed with ethanol, and dried at 70 °C in an oven overnight. The UiO-66-NH_2-$ILPF_6^-$-guanidine was reused four times without a significant loss in its catalytic activity (Fig. 8). The slight reduction in the catalyst performance could be related to the loss of the catalyst within the recycling process, proved by ICP-OES. However, the remained catalyst activity indicates the high structural stability of the catalyst. The stability of UiO-66-NH_2-$ILPF_6^-$-guanidine heterogeneous catalyst was evaluated by XRD, FTIR, and SEM/elemental mapping. The XRD pattern of the recovered catalyst (after four times reused) indicates that the crystal structure of the framework has been preserved (Fig. 1). The FTIR spectrum showed that the catalyst retained its structure after four times reusing (Fig. 2). The SEM image and elemental mapping exhibited that the morphology of the particles and the elemental distribution in the structure of the catalyst was remained unchanged after four times reusing the catalyst (Fig. S6).

Moreover, the stability of the catalyst, UiO-66-NH_2-$ILPF_6^-$-guanidine, was examined by the leaching test. The test was performed for the model reaction in two steps (Fig. S7) In the first step, the catalyst was separated from the reaction medium by centrifugation after 10 min and the reaction let be continued until 45 min in the absence of the catalyst. A reaction yield of 20% was obtained. The content of

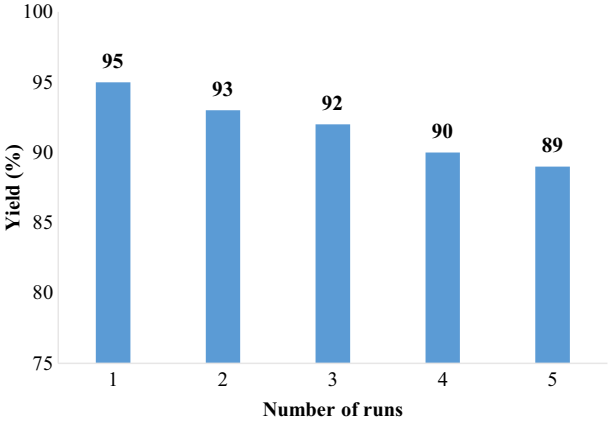

Fig. 8 Reusability of the catalyst

Table 5 Comparison study in the synthesis of the xanthene with benzaldehyde (1 mmol) and dimedone (2 mmol) in the presence of different catalytic systems

Entry	Catalyst	Conditions	Time (min)	Yield (%)[Ref]
1	Cu/Cr-MIL-101 (0.05 g)	120 °C, solvent-free	2 (h)	94 [55][a]
2	Fe–Mg MOF (0.05 g)	120 °C, solvent-free	2 (h)	93 [56][a]
3	Fe_3O_4@THAM-piperazine (0.01 g)	H_2O/EtOH (1:1), reflux	15	88 [51]
4	BTMA-Br_3 (0.1 g)	MW, Solvent-free	5	96 [53]
5	1,1′-Butylenebis(3-sulfo-3H-imidazol-1-ium) chloride (2 mL)	50 °C	10	91 [52]
6	4-[3-(4-Sulfo-butyl)-imidazol-1-yl]-butane-1-sulfonate (0.2 mL)	50 °C	30	91 [58]
7	Perlite nanoparticles@IL/$ZrCl_4$ (0.005 g)	80 °C, solvent-free	100	92 [54][a]
8	Fe_3O_4@Propylsilane-Histidine[HSO_4^-] (0.08 g)	reflux, EtOH	5	92 [57]
9	UiO-66-NH_2-ILPF_6^--guanidine (0.03 g)	rt/EtOH	45	95 [Present work]

[a]Precursor: 3-Nitrobenzaldehyde

zirconium in the recovered catalyst was found to be 5.70 mol%, determined according to the method described in the literature [69]. A slight decrease in the zirconium content, compared to the content in the fresh catalyst (6 mmol%), might be related to the inevitable detriment in catalyst recycling and regenerating (i.e., centrifugation and rinsing with solvents). In the second step, the catalyst was removed after 25 min and the reaction continued till 45 min, and a yield of ~ 50% was found. The zirconium content was also determined as 5.11 mol% in the recovered catalyst. A comparison between these results and the results in the optimized conditions (95% yield within 45 min) indicates that the leaching of the guanidine did not happen, which could catalyze the reaction after removal of the catalyst.

The performance of our catalyst was compared with other catalytic systems such as MOFs, ILs, and supported ILs, reported in the literature recently (Table 5) [51–58]. The MOFs (entries 1 and 2) as heterogeneous catalysts exhibited great catalytic activity in high temperatures, solvent-free conditions, and long reaction times. The ILs (entries 3–6) as homogeneous catalysts/media showed good yields, without the utilization of additional solvent, in temperatures higher than room temperature, in short reaction times. The nanoparticle-supported ILs (heterogeneous catalysts) exhibited good performance in elevated temperatures (entries 7 and 8). In the present work, the synthesis was carried out in non-toxic/non-volatile solvent and room temperature with high yield. Our catalytic system showed comparable efficiency with reported results and proving milder conditions in temperature and reaction medium.

Conclusion

A supported ionic liquid catalyst was presented for the synthesis of xanthenes. The basic heterogeneous catalyst was prepared by the functionalization of Zr-based MOF with an ionic liquid. Guanidine was then attached to the ionic liquid, along with an anion exchange by replacing Br^- with PF_6^-. Various types of aldehydes were successfully reacted with dimedone to produce xanthenes in good to high yield in the presence of the catalyst. The type of solvent, temperature, and catalyst amount were effective parameters in the reaction. Furthermore, a synergistic effect between the MOF and the IL/guanidine was observed. The catalyst was capable of recycling and reuse several times. The stability of the catalyst was confirmed by XRD, FTIR, SEM/elemental mapping, and also leaching test. It is expected that such a hybrid system, MOF/IL/organocatalyst, finds further development and deep understanding to know the role of each catalyst component in the organic synthesis. Moreover, the high surface area and porosity of MOFs provide a great opportunity for organocatalysts to stabilize on the surface of porous materials and generate a unique heterogeneous catalytic system.

Supplementary Information The online version contains supplementary material available at https://doi.org/10.1007/s11164-021-04439-1.

Acknowledgements The authors gratefully acknowledge Razi University for financial support.

References

1. C. Dai, J. Zhang, C. Huang, Z. Lei, Chem. Rev. **117**, 6929 (2017)
2. J.P. Hallett, T. Welton, Chem. Rev. **111**, 3508 (2011)
3. B. Xin, J. Hao, Chem. Soc. Rev. **43**, 7171 (2014)
4. Q.-X. Luo, B.-W. An, M. Ji, J. Zhang, Mater. Chem. Front. **2**, 219 (2018)
5. B.V. Romanovsky, I.G. Tarkhanova, Russ. Chem. Rev. **86**, 444 (2017)
6. L. Jiao, J.Y.R. Seow, W.S. Skinner, Z.U. Wang, H.-L. Jiang, Mater. Today. **27**, 43 (2019)
7. V. Pascanu, G.G. Miera, A.K. Inge, B. Martín-Matute, J. Am. Chem. Soc. **141**, 7223 (2019)
8. H. He, J.A. Perman, G. Zhu, S. Ma, Small **12**, 6309 (2016)
9. J. Gascon, A. Corma, F. Kapteijn, F.X. Llabrés i Xamena, ACS Catal. **4,** 361 (2014)
10. D. Farrusseng, S. Aguado, C. Pinel, Angew. Chem. Int. Ed. **48**, 7502 (2009)
11. C. Doonan, R. Riccò, K. Liang, D. Bradshaw, P. Falcaro, Acc. Chem. Res. **50**, 1423 (2017)
12. W. Cai, C.-C. Chu, G. Liu, Y.-X.J. Wáng, Small **11**, 4806 (2015)
13. R.J. Kuppler, D.J. Timmons, Q.-R. Fang, J.-R. Li, T.A. Makal, M.D. Young, D. Yuan, D. Zhao, W. Zhuang, H.-C. Zhou, Coord. Chem. Rev. **253**, 3042 (2009)
14. D. Yang, B.C. Gates, ACS Catal. **9**, 1779 (2019)
15. S.M.J. Rogge, A. Bavykina, J. Hajek, H. Garcia, A.I. Olivos-Suarez, A. Sepúlveda-Escribano, A. Vimont, G. Clet, P. Bazin, F. Kapteijn, M. Daturi, E.V. Ramos-Fernandez, F.X. Llabrés i Xamena, V. Van Speybroeck, J. Gascon, Chem. Soc. Rev. **46,** 3134 (2017)
16. A. Dhakshinamoorthy, A.M. Asiri, H. Garcia, Catal. Sci. Technol. **6**, 5238 (2016)
17. P. Valvekens, F. Vermoortele, D. De Vos, Catal. Sci. Technol. **3**, 1435 (2013)
18. F. Zhang, S. Zheng, Q. Xiao, Y. Zhong, W. Zhu, A. Lin, M.S. El-Shall, Green Chem. **18**, 2900 (2016)
19. P. Falcaro, R. Ricco, A. Yazdi, I. Imaz, S. Furukawa, D. Maspoch, R. Ameloot, J.D. Evans, C.J. Doonan, Coord. Chem. Rev. **307**, 237 (2016)
20. A. Dhakshinamoorthy, A. Santiago-Portillo, A.M. Asiri, H. Garcia, ChemCatChem **11**, 899 (2019)
21. J. Wang, M. Yang, W. Dong, Z. Jin, J. Tang, S. Fan, Y. Lu, G. Wang, Catal. Sci. Technol. **6**, 161 (2016)
22. C.-D. Wu, M. Zhao, Adv. Mater. **29**, 1605446 (2017)
23. D. Ma, B. Li, K. Liu, X. Zhang, W. Zou, Y. Yang, G. Li, Z. Shi, S. Feng, J. Mater. Chem. A **3**, 23136 (2015)
24. N.A. Khan, Z. Hasan, S.H. Jhung, Chem. Eur. J. **20**, 376 (2014)
25. K. Fujie, H. Kitagawa, Coord. Chem. Rev. **307**, 382 (2016)
26. B. Mirhosseini-Eshkevari, M.A. Ghasemzadeh, M. Esnaashari, Appl. Organomet. Chem. **33**, e5027 (2019)
27. A. Dhakshinamoorthy, A.M. Asiri, M. Alvaro, H. Garcia, Green Chem. **20**, 86 (2018)
28. M. Ding, H.-L. Jiang, ACS Catal. **8**, 3194 (2018)
29. L.-G. Ding, B.-J. Yao, W.-L. Jiang, J.-T. Li, Q.-J. Fu, Y.-A. Li, Z.-H. Liu, J.-P. Ma, Y.-B. Dong, Inorg. Chem. **56**, 2337 (2017)
30. Z. Wu, C. Chen, H. Wan, L. Wang, Z. Li, B. Li, Q. Guo, G. Guan, Energy Fuels **30**, 10739 (2016)
31. L. Peng, J. Zhang, S. Yang, B. Han, X. Sang, C. Liu, G. Yang, Green Chem. **17**, 4178 (2015)
32. B. Mirhosseini-Eshkevari, M.A. Ghasemzadeh, M. Esnaashari, S. Taghvaei Ganjali, ChemistrySelect **44,** 12920 (2019)
33. S. Chong, T. Wang, H. Zhong, L. Xu, H. Xu, Z. Lv, M. Ji, Green. Energy Environ. **5**, 154 (2020)
34. M. Jin, Q. Niu, G. Liu, Z. Lv, C. Si, H. Guo, J. Mater. Sci. **55**, 8199 (2020)
35. C. Chen, Z. Wu, Y. Que, B. Li, Q. Guo, Z. Li, L. Wang, H. Wan, G. Guan, RSC Adv. **6**, 54119 (2016)
36. M. Nandi, J. Mondal, K. Sarkar, Y. Yamauchi, A. Bhaumik, Chem. Commun. **47**, 6677 (2011)
37. B. Maleki, A. Davoodi, M.V. Azghandi, M. Baghayeri, E. Akbarzadeh, H. Veisi, S.S. Ashrafi, M. Raei, New J. Chem. **40**, 1278 (2016)
38. J. Mondal, M. Nandi, A. Modak, A. Bhaumik, J. Mol. Catal. A **363**, 254 (2012)
39. S.N.K. Mogha, K. Chaudhary, G. Kumar, D.T. Masram, ACS Omega **3**, 16377 (2018)
40. E. Rostami, S.H. Zare, ChemistrySelect **4**, 13295 (2019)
41. I. Pugazhenthi, S.M. Ghouse, F.-R. Nawaz Khan, E.D. Jeong, J.S. Bae, J.-P. Kim, E.H. Chung, Y.S. Kumar, C. Dasaradhan, RSC Adv. **5,** 17257 (2015)
42. A. Bamoniri, B.B.F. Mirjalili, S. Fouladgar, Polycycl. Aromat. Compd. **37**, 345 (2017)

43. M.A. Ghasemzadeh, F. Ghaffarian, Appl. Organomet. Chem. **34**, e5580 (2020)
44. M.M. Reddy, A. Sivaramakrishna, ChemistrySelect **5**, 4816 (2020)
45. D. Zhu, M. Li, Z. Wu, Y. Du, B. Luo, P. Huang, S. Wen, Eur. J. Org. Chem. **28**, 4566 (2019)
46. S. Sadjadi, F.G. Kahangi, M. Dorraj, M.M. Heravi, Molecules **25**, 241 (2020)
47. K.D. Safa, E. Taheri, M. Allahvirdinesbat, A. Niaei, Res. Chem. Intermed. **42**, 2989 (2016)
48. K. Tabatabaeian, M.A. Zanjanchi, M. Mamaghani, A. Dadashi, Res. Chem. Intermed. **42**, 5049 (2016)
49. B. Zeynizadeh, S. Rahmani, RSC Adv. **9**, 28038 (2019)
50. V.B. Nishtala, S. Basavoju, Synth. Commun. **49**, 2342 (2019)
51. N. Mulakayala, G.P. Kumar, D. Rambabu, M. Aeluri, M.V. Basaveswara Rao, Tetrahedron Lett. **53,** 6923 (2012)
52. N.G. Khaligh, Res. Chem. Intermed. **44**, 4045 (2018)
53. P. Ramakanth, K. Uppalaiah, Org. Prep. Proced. Int. **1** (2020)
54. L. Moradi, M. Mirzaei, RSC Adv. **9**, 19940 (2019)
55. S.M. El-Dafrawy, R.S. Salama, S.A. El-Hakam, S.E. Samra, J. Mater. Res. Technol. **9**, 1998 (2020)
56. W.S. Abo El-Yazeed, Y.G. Abou El-Reash, L.A. Elatwy, A.I. Ahmed, RSC Adv. **10,** 9693 (2020)
57. S.M. Mousavifar, H. Kefayati, S. Shariati, Appl. Organomet. Chem. **32**, e4242 (2018)
58. N.G. Khaligh, L.S. Teng, O.C. Ling, M.R. Johan, J.J. Ching, J. Mol. Liq. **278**, 19 (2019)
59. S. Askari, M. Jafarzadeh, D.B. Christensen, S. Kegnæs, Catal. Lett. **150**, 3159 (2020)
60. W. Peng, P. Hao, J. Luo, B. Peng, X. Han, H. Liu, Ind. Eng. Chem. Res. **59**, 4273 (2020)
61. M. Kandiah, M.H. Nilsen, S. Usseglio, S. Jakobsen, U. Olsbye, M. Tilset, C. Larabi, E.A. Quadrelli, F. Bonino, K.P. Lillerud, Chem. Mater. **22**, 6632 (2010)
62. C.S. Hinde, W.R. Webb, B.K.J. Chew, H.R. Tan, W.-H. Zhang, T.S.A. Hor, R. Raja, Chem. Commun. **52**, 6557 (2016)
63. J.F. Kurisingal, Y. Rachuri, R.S. Pillai, Y. Gu, Y. Choe, D.-W. Park, Chemsuschem **12**, 1033 (2019)
64. M. Thommes, K. Kaneko, A.V. Neimark, J.P. Olivier, F. Rodriguez-Reinoso, J. Rouquerol, K.S.W. Sing, Pure Appl. Chem. **87**, 1051 (2015)
65. B. Karami, S.J. Hoseini, K. Eskandari, A. Ghasemi, H. Nasrabadi, Catal. Sci. Technol. **2**, 331 (2012)
66. F. Darviche, S. Balalaie, F. Chadegani, Synth. Commun. **37**, 1059 (2007)
67. A. Hasaninejad, M. Dadar, A. Zare, Chem. Sci. Trans. **1**, 233 (2012)
68. B.R. Madje, M.B. Ubale, J.V. Bharad, M.S. Shingare, S. Afr, J. Chem. **63**, 36 (2010)
69. H. Chen, L. Fan, X. Zhang, A.C.S. Appl, Mater. Interfaces **12**, 54884 (2020)